







**Three-dimensional quasi-quantized Hall insulator phase in SrSi<sub>2</sub>**

K. Manna <sup>1,2,\*</sup>, N. Kumar <sup>2,3</sup>, S. Chattopadhyay <sup>4</sup>, J. Noky<sup>2</sup>, M. Yao<sup>2</sup>, J. Park<sup>4</sup>, T. Förster<sup>4</sup>, M. Uhlarz<sup>4</sup>, T. Chakraborty<sup>2</sup>, B. V. Schwarze <sup>4</sup>, J. Hornung<sup>4</sup>, V. N. Strocov <sup>5</sup>, H. Borrmann<sup>2</sup>, C. Shekhar <sup>2</sup>, Y. Sun<sup>2</sup>, J. Wosnitza<sup>4,6</sup>, C. Felser<sup>2</sup> and J. Gooth<sup>2,6,†</sup>

<sup>1</sup>Indian Institute of Technology-Delhi, Hauz Khas, New Delhi 110 016, India

<sup>2</sup>Max Planck Institute for Chemical Physics of Solids, Nöthnitzer Straße 40, 01187 Dresden, Germany

<sup>3</sup>S. N. Bose National Centre for Basic Sciences, Salt Lake City, Kolkata 700 106, India

<sup>4</sup>Hochfeld-Magnetlabor Dresden (HLD-EMFL) and Würzburg-Dresden Cluster of Excellence *ct.qmat*, Helmholtz-Zentrum Dresden-Rossendorf, 01328 Dresden, Germany

<sup>5</sup>Swiss Light Source, Paul Scherrer Institut, CH-5232 Villigen PSI, Switzerland

<sup>6</sup>Institut für Festkörper- und Materialphysik, Technische Universität Dresden, 01062 Dresden, Germany



(Received 29 July 2021; revised 3 December 2021; accepted 14 June 2022; published 18 July 2022)

In insulators, the longitudinal resistivity becomes infinitely large at zero temperature. For classical insulators, the Hall conductivity becomes zero at the same time. However, there are special systems, such as two-dimensional quantum Hall insulators, in which a more complex scenario is observed at high magnetic fields. Here, we report experimental evidence for a quasi-quantized Hall insulator in the quantum limit of the three-dimensional compound SrSi<sub>2</sub>. Our measurements reveal a magnetic-field range, in which the longitudinal resistivity diverges with decreasing temperature, while the Hall conductivity approaches a quasi-quantized value that is given only by the conductance quantum and the Fermi wave vector in the field direction. The quasi-quantized Hall insulator appears in a magnetic field induced insulating ground state of three-dimensional materials and is deeply rooted in quantum Hall physics.

DOI: [10.1103/PhysRevB.106.L041113](https://doi.org/10.1103/PhysRevB.106.L041113)

**Introduction.** The quantum Hall insulator (QHI) is one of the ground states in two-dimensional (2D) electron systems exposed to a strong magnetic field  $B$ . It is characterized by a diverging longitudinal resistivity ( $\rho_{xx} \rightarrow \infty$ ) as  $T \rightarrow 0$  and a finite Hall conductivity ( $\sigma_{xy}$ ) that approaches the value  $e^2/h$  containing only fundamental constants: the elementary charge  $e$  and the Planck's constant  $h$  [1–7]. This state differs fundamentally from a classical insulator for which  $\rho_{xx}$  diverges and  $\sigma_{xy}$  vanishes at zero temperature [8–12].

The QHI state usually occurs in between two other ground states of 2D systems. The first is the quantum Hall liquid (QHL) state [13,14], which is characterized by a vanishing  $\rho_{xx}$  and a quantized  $\sigma_{xy} = \nu e^2/h$ , where  $\nu$  is a rational number ( $\rho_{xx} \rightarrow 0$  and  $\sigma_{xy} \rightarrow \nu e^2/h$  as  $T \rightarrow 0$ ). The second is the ordinary Hall insulator (HI) state [15], which is characterized by a diverging  $\rho_{xx}$  and  $\sigma_{xy} \approx en/B$  where  $n$  is the density of electrons in zero magnetic field [ $\rho_{xx}(B) \rightarrow \infty$  and  $\sigma_{xy}(B) \rightarrow en/B$  as  $T \rightarrow 0$ ]. By changing the applied magnetic field and/or disorder, it is possible to drive transitions between the different ground states and to thereby study the quantum critical phenomena associated with them [1,8].

In a three-dimensional (3D) electron system,  $\sigma_{xy}$  is never truly quantized [16–18]. Recently, however, a 3D relative of the QHL was reported as the quasi-quantized Hall effect in the Dirac semimetals ZrTe<sub>5</sub> [19,20] and HfTe<sub>5</sub> [21,22], and in

doped InAs [23]. The characteristic of the 3D quasi-quantized Hall effect, i.e., the 3D quasi-quantized Hall liquid (QQHL), in the quantum limit (where only the lowest Landau band is occupied) is that  $\sigma_{xy}$  is given by only the conductance quantum  $e^2/h$ , scaled by the Fermi wave vector  $k_F$  of electrons along  $B$  [ $\sigma_{xy}(B) \rightarrow (e^2/h)k_F/\pi$  as  $T \rightarrow 0$ ], while  $\rho_{xx}$  approaches a finite, nonquantized value for  $T \rightarrow 0$ . The value of  $\rho_{xx}$  depends on sample details, such as the residual resistivity at low temperatures. Importantly, the QHL and QQHL have a common origin: Both phases are directly related to the Berry curvature of the electron states in their respective dimension [16]. This naturally raises the question of whether relatives of the insulating ground states associated with the quantum Hall regime in two dimensions might also occur in 3D systems.

In fact, a  $B$ -driven transition between a QQHL and 3D HI has recently been observed deep in the quantum limit of ZrTe<sub>5</sub> [19,20] and HfTe<sub>5</sub> [21,22], and in doped InAs [23]. However, the transition from the QQHL to the 3D HI through a quasi-quantized Hall insulator (QQHI) phase [ $\rho_{xx}(B) \rightarrow \infty$  and  $\sigma_{xy}(B) \rightarrow (e^2/h)k_{F,z}/\pi$  as  $T \rightarrow 0$ ], i.e., the 3D equivalent of the 2D QHI, has rarely been observed. Here, we report the QQHI state in a 3D compound SrSi<sub>2</sub>, containing near-spherical Fermi surfaces.

SrSi<sub>2</sub> crystallizes in the chiral space group  $P4_132$  (No. 213) with a helical arrangement of Si atoms along the (111) direction [Fig. 1(a)]. Originally, SrSi<sub>2</sub> was predicted to be a Weyl semimetal with a higher Chern number of  $\pm 2$  [24,25]. Nevertheless, recent angle-resolved photoemission spectroscopy (ARPES) measurements reveal that SrSi<sub>2</sub> exhibits only trivial

\*Kaustuv.Manna@physics.iitd.ac.in

†johannes.gooth@cpfs.mpg.de

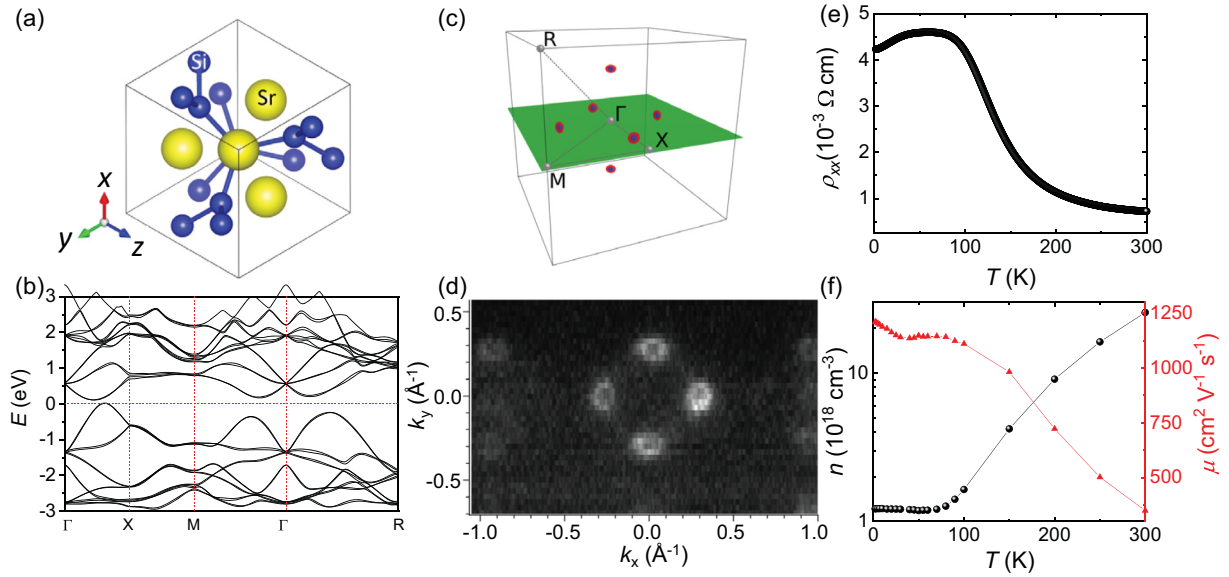


FIG. 1. (a) Crystal structure of SrSi<sub>2</sub> with chiral space group  $P4_132$  (No. 213). (b) Trivial band structure of SrSi<sub>2</sub> in agreement with a recent ARPES study [26]. (c) Six pairs of spin-split hole Fermi-surface pockets in the BZ along  $\pm k_x$ ,  $\pm k_y$ , and  $\pm k_z$ . (d) Constant energy surface at  $E_F$  and  $k_z = 0$  measured by ARPES acquired with a photon energy  $h\nu = 342$  eV. Cross sections of a set of four near-spherical Fermi-surface pockets lying in the  $k_x$ - $k_y$  plane are clearly visible. The corresponding plane is highlighted in green in (c). (e) Temperature-dependent resistivity of SrSi<sub>2</sub> with current passed along [100] in the absence of a magnetic field. (f) Temperature-dependent charge-carrier concentration ( $n$ ) and mobility ( $\mu$ ) of SrSi<sub>2</sub> estimated using the low magnetic field slope of  $\rho_{yx}(B)$ .

pockets with a parabolic dispersion at the Fermi energy  $E_F$  [26]. *Ab initio* calculations using density-functional theory [27–29] of the band structure [Fig. 1(b)] show a global band gap of  $\sim 100$  meV, making SrSi<sub>2</sub> a semiconductor. However,  $E_F$  is located slightly below the tip of the valence band which results in small Fermi pockets in the first Brillouin zone (BZ); see Fig. 1(c). The lack of inversion symmetry in SrSi<sub>2</sub> leads to six spin-split pairs of nearly spherical hole pockets distributed in the momentum space directions  $\pm k_x$ ,  $\pm k_y$ , and  $\pm k_z$  along the high-symmetry lines  $\Gamma$ - $X$ . The larger Fermi-surface pocket (red) is labeled  $\beta$ , whereas its spin-split counterpart, the smaller Fermi-surface (FS) pocket (blue) is labeled  $\alpha$ .

*Experiment and analysis.* All single-crystalline samples used in our study were grown via the optical floating zone technique (see Supplemental Material [30]). Detailed single-crystal diffraction experiments and analysis were performed on the grown crystals. The crystal structure is found to be  $P4_132$  (No. 213) chiral type, with Flack parameters  $\sim 0.016(12)$ , confirming a single-handed chiral domain structure in the grown crystals. Figure 1(d) shows an ARPES (also see Supplemental Material [30]) image of the  $k_x$ - $k_y$  plane taken from one of these samples. Here, the ARPES experiments on the SrSi<sub>2</sub> single crystals were conducted using soft x-ray ARPES (SXARPES) at the ADDRESS beamline of the Swiss Light Source using a SPECS analyzer [31,32]. Although the spin splitting between the  $\alpha$  and  $\beta$  pockets is beyond the experimental resolution, the observed projection of four Fermi-surface pockets located at  $\pm k_x$  and  $\pm k_y$  is consistent with the band-structure calculations.

For the electrical-transport experiments, several millimeter-size rectangular SrSi<sub>2</sub> single-crystalline bars were prepared such that the edges of the bars were aligned

along the crystallographic directions (crystals containing {100} planes or crystals with their length along [110], width along [111], and height along  $[-112]$ , etc.), that correspond to the indexes  $x$ ,  $y$ , and  $z$  of the transport coefficients. On bars aligned in this way, we measured  $\rho_{xx}$  and  $\rho_{yx}$  with a standard four-probe low-frequency lock-in technique in DC and pulsed magnetic fields at various  $T$  (see Supplemental Material [30]). At  $B = 0$ ,  $\rho_{xx}$  and  $n$  exhibit the typical behavior of an intrinsically doped semiconductor [Figs. 1(e) and 1(f)] [33].  $\rho_{xx}$  increases with increasing  $T$ , while  $n$  remains nearly constant up to 75 K, indicating a metallic regime. Around 75 K, however, thermal activation across the band gap sets in, causing the charge-carrier concentration  $n$  to increase with increasing  $T$  and  $\rho_{xx}$  to decrease.  $d\rho_{yx}(B)/dB$  is positive below 75 K, indicating hole-dominated transport in the metallic temperature regime, which agrees with our band-structure calculations and ARPES experiments. An important detail that distinguishes our study from past experiments on the quasiquantized 3D Hall regime is that our samples have a much lower charge-carrier mobility  $\mu$  [Fig. 1(f)]. At 2 K, we estimate  $\mu = 1.21 \times 10^3 \text{ cm}^2 \text{ V}^{-1} \text{ s}^{-1}$ , which is approximately two orders of magnitude lower than the charge-carrier mobility for ZrTe<sub>5</sub> [19,20] and HfTe<sub>5</sub> [21,22], and in doped InAs [23]. This is a key difference because in 2D systems, the transition to the QHI is tied to samples with particularly low  $\mu$ , in which incoherent scattering dominates [8].

To characterize the FS morphology of our samples, we measured Shubnikov–de Haas (SdH) oscillations [34] with respect to the main crystal axes at 2 K [Fig. 2(a)]. We found two fundamental SdH frequencies [Fig. 2(b)] that do not change for different field alignments within the experimental resolution [Figs. 2(c) and 2(d)], which is consistent with two 3D

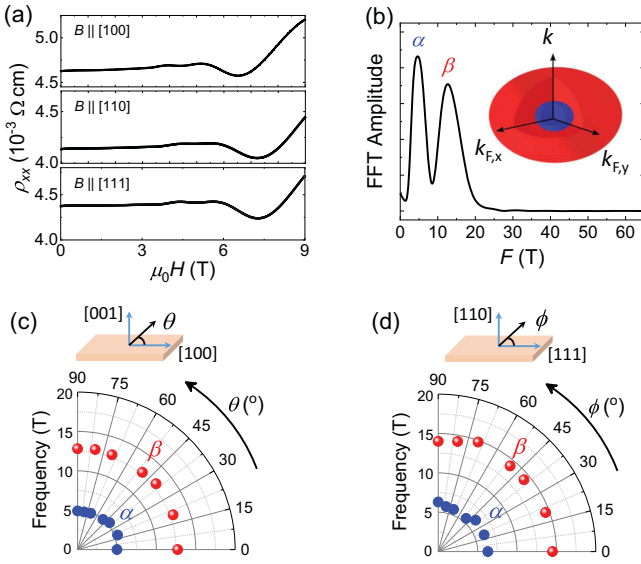


FIG. 2. (a) Shubnikov–de Haas (SdH) oscillations at 2 K with a magnetic field applied along important cubic crystallographic directions: [100], [110], and [111], which exhibit nearly identical quantum oscillations. (b) Fast Fourier transform (FFT) amplitudes for SrSi<sub>2</sub> determined from SdH oscillations for  $B$  along [100]. The inset shows the near-spherical Fermi-surface pockets predicted by the calculations. (c,d) Angle-dependent SdH oscillations with nearly identical oscillation frequencies that are in agreement with the nearly spherical Fermi-surface pockets in SrSi<sub>2</sub> are revealed.

spherical Fermi-surface pockets of different sizes. Based on the *ab initio* band-structure calculations, we assigned the obtained frequencies  $f_\alpha = 5.3$  T and  $f_\beta = 12.8$  T to the  $\alpha$  and  $\beta$  pocket, respectively. The corresponding zero-field Fermi wave vectors  $k_{F,0,i}$  ( $i = \alpha, \beta$ ) were then estimated using the Onsager relation  $k_{F,0,i} = \sqrt{f_i 4\pi e/h}$ , yielding  $k_{F,0,\alpha} = 0.013 \text{ \AA}^{-1}$  and  $k_{F,0,\beta} = 0.020 \text{ \AA}^{-1}$ . Further details of the band-structure analysis can be found in Fig. S2 in the Supplemental Material [30]. We want to explicitly point out two results of this analysis: The quantum limits for the  $\alpha$  and  $\beta$  pockets in our SrSi<sub>2</sub> samples have already been reached for fields of  $B_{QL,\alpha} \approx 5.3$  T and  $B_{QL,\beta} \approx 12.8$  T, respectively, and the  $\alpha$  pockets are already completely gapped out above  $B_{G,\alpha} \approx 11.4$  T (see Supplemental Material [30]). Thus, above  $B_{QL,\beta}$ , all charge carriers are in the lowest Landau band of the  $\beta$  pockets.

We now identify the different phases in SrSi<sub>2</sub> above  $B_{QL,\beta}$  at low temperatures. More precisely, we measured in the configuration of the magnetic field aligned along the  $z$  axis ( $B_z$ ). Experimental identification of an insulating or metallic phase is based on extrapolation of the measured  $\rho_{xx}$  in  $B$  and at a finite temperature to  $T = 0$ . However, if  $\rho_{xx}$  increases (exponentially) with decreasing  $T$ , the state is usually considered to be an insulator. Conversely, if  $\rho_{xx}$  decreases with decreasing  $T$ , the state is regarded as a metal. In a 2D electron system, the transition between an insulating phase and a metallic phase in the quantum Hall regime can be characterized by a critical magnetic-field value  $B_c$ , for which  $\rho_{xx}$  is  $T$  independent and where the derivative of the  $T$  dependence changes sign on each side of the transition [35]. In experiments,  $B_c$  is usually extracted from the intersection of  $\rho_{xx}(B)$  curves measured at

various values of  $T$  [1]. The transition between the QQHL and HI in the 3D quasiquantized Hall regime has been characterized in a similar way in ZrTe<sub>5</sub> [19].

Following this procedure, we plot  $\rho_{xx}(B)$  and  $\sigma_{xy}(B)$  of our SrSi<sub>2</sub> sample for various  $T$  in Figs. 3(a) and 3(b), respectively. Starting from low fields, we find that SrSi<sub>2</sub> enters the metallic 3D QQHL phase [16] just above  $B_{QL,\alpha}$ . In this phase,  $\rho_{xx}$  decreases monotonically with decreasing  $T$  [Fig. 3(c)], approaching a finite, nonquantized value, whereas  $\sigma_{xy}$  converges to  $6(e^2/h)k_F/\pi$  for  $T \rightarrow 0$  [Figs. 3(b) and 3(d)]. The sixfold degeneracy of  $\sigma_{xy}$  comes from the six  $\beta$  pockets in the Brillouin zone (BZ). For 3D systems with a parabolic band structure,  $k_F$  of the lowest Landau band is  $B$  dependent [16,23]. In particular,  $k_F = \sqrt{k_{F,0}^2 - 2eB/h}$ . Consequently, in SrSi<sub>2</sub> the quasiquantized Hall conductivity above  $B_{QL,\beta}$  in the zero- $T$  limit is given by  $\sigma_{xy} = \frac{6e^2}{h} \sqrt{k_{F,0,\beta}^2 - 2eB/h}/\pi$ . With increasing  $B$ , a transition at  $B_c \approx 20.2$  T from the QQHL to an insulating phase can be identified in the intersection of the  $\rho_{xx}$  curves obtained at different values of  $T$  in Fig. 3(a). In the insulating phase [Fig. 3(d)], a striking observation can be made: Just above  $B_c$ , there is a field range of approximately 2 T in which  $\sigma_{xy}$  remains quasiquantized up to approximately  $B_T = 22.2$  T. Beyond  $B_T$ ,  $\sigma_{xy}$  deviates from the theoretical single-particle model with a fixed Fermi energy as shown in Fig. 3(b). Between  $B_c$  and  $B_T$ , the deviation of  $\sigma_{xy}$  from  $6(e^2/h)k_{F,\beta}/\pi$  at 0.6 K is less than 1%, even though  $\rho_{xx}(B)$  increases monotonically for  $T \rightarrow 0$ . This reflects the expected features of a magnetic field tuned 3D QQHI phase.

Theoretically, the magnetic field driven transitions from a liquid phase to an insulating phase in the quantum Hall or quasiquantized Hall regime are considered to be transitions between delocalized and localized phases [8–12,36,37]. They can be understood in the context of percolation path network models, which provide similar results in two [8–12] and three [38,39] dimensions. The insulating phases are not entirely insulating in their bulk but are rather described as separate clusters of liquid states that exist in potential minima induced by random impurities and defects throughout the samples. Since the electrons are effectively localized within these clusters, the localization length can then be defined as the correlation length—the width of the electron clusters  $\lambda_1$ . As the critical magnetic field  $B_c$  found at the center of a Landau-level band is approached, percolation theory states that  $\lambda_1$ , i.e., the size of the clusters, increases according to the power law,

$$\lambda_1 \propto |B - B_c| T^{-1/\zeta},$$

with the universal critical exponent  $\zeta$ . As the critical point or percolation threshold  $B_c$  is approached, the clusters grow in size, merging together, and then begin to form extended clusters of larger sizes, until at the percolation threshold, enough clusters merge to form a percolating equipotential which extends across the entire system.

The transport is then obtained via a scattering matrix, which parametrizes the tunneling of electrons (holes) from one liquid cluster to the other, leading to the diverging  $\rho_{xx}$  for  $T \rightarrow 0$ . When the phase coherence of the electron (hole)

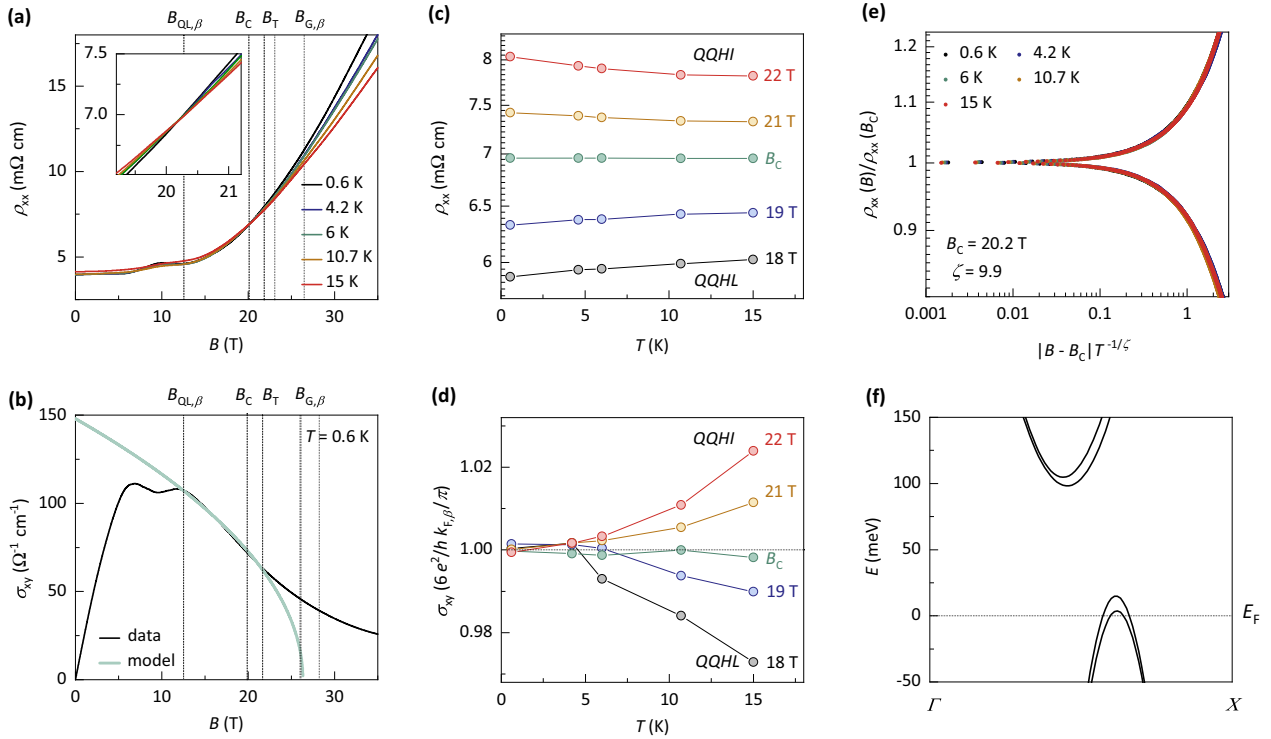


FIG. 3. (a) Longitudinal resistivity  $\rho_{xx}$  as a function of magnetic field  $B$  for various temperatures  $T$ . The field at which the  $\beta$  pocket enters the quantum limit (the lowest Landau band) is denoted by  $B_{QL,\beta}$ .  $B_c$  marks the transition point from a metallic to an insulating state. (b) Hall conductivity  $\sigma_{xy}$  as a function of  $B$  at  $T = 0.6$  K. In the insulating phase, between  $B_c$  and  $B_T$ , the experimentally determined  $\sigma_{xy}$  (black curve) scales with the calculated 3D quasi-quantized Hall conductivity value (light green curve) estimated using the experimentally extracted Fermi wave vector  $k_F$  along  $B$ , the electron charge  $e$ , and the Planck constant  $h$ . The thickness of the light green line represents the error of the model, originating from a statistical error of 1% in  $k_F$ .  $B_{G,\beta}$  marks the theoretical field at which SrSi<sub>2</sub> hypothetically enters the band gap. Further detailed descriptions of the highlighted magnetic-field values can be found in the Supplemental Material [30]. (c)  $\rho_{xx}$  as a function of  $T$  for various  $B$  around  $B_c$ . (d)  $\sigma_{xy}$  as a function of  $T$  for various  $B$  around  $B_c$ . (e) Normalized resistivity,  $\rho_{xx}(B)/\rho_{xx}(B_c)$ , as a function of the scaling parameter  $|B - B_c|T^{-1/\zeta}$ , with the critical exponent  $\zeta = 9.9$ . (f) Zoomed-in view of the band structure of SrSi<sub>2</sub>, revealing two hole pockets.

wave functions is maintained after each tunneling event, the insulating states are ordinary HIs [38,40,41]. Conversely, for 2D systems it has been shown that if the phase coherence of the electron (hole) wave functions is destroyed after each tunneling event,  $\sigma_{xy}$  is quantized; i.e., the system is a QHI [40]. A similar mechanism may distinguish the ordinary HI from the QQHI phase in 3D systems.

The isotherms of  $\rho_{xx}$  for such magnetic field induced metal-insulator transitions typically scale with  $\lambda_1$  and thus obey a universal scaling law with the parameter  $(B - B_c)T^{-1/\zeta}$ . This applies to transitions between the QHL and QHI in 2D systems [35] as well as to transitions between the 3D QQHL and the ordinary HI [38,40], as in ZrTe<sub>5</sub> [19]. In Fig. 3(e), we show such a scaling analysis for SrSi<sub>2</sub> above  $B_{QL,\beta}$ , and indeed find that all isotherms of  $\rho_{xx}$  fall on a single curve as a function of  $(B - B_c)T^{-1/\zeta}$  for  $\zeta \approx 9.9$ .

Deeper in the insulating state, we observe that  $\sigma_{xy}$  begins to deviate from its quasi-quantized value, and the state seems to evolve continuously towards a 3D HI. We define the crossover between these insulating states by a transition field  $B_T$ , at which the experimentally determined  $\sigma_{xy}$  deviates more than 1% from  $6(e^2/h)k_{F,\beta}/\pi$ . The crossover can be understood as a field-driven change from a state of constant Fermi level  $E_F$  to a state at which  $E_F$  is not strictly fixed anymore [20,21,23]. The considerations presented above strongly depend on  $E_F$  being

fixed, which ensures that the lowest Landau bands shift linearly with  $B$ . In materials with relatively small Fermi-surface areas, such as SrSi<sub>2</sub>, such a situation can occur as a result of defect states that absorb some of the conduction electrons (holes), thereby ensuring overall charge neutrality. However, the number of these defect states in real samples is limited. Moreover, as soon as the defect states are fully occupied,  $E_F$  begins to move with  $B$  to avoid large charging energies and  $\sigma_{xy}$  approaches its classical value. In agreement with our observations, such a crossover usually occurs in large fields as the bottom of the last populated Landau band approaches  $E_F$ . In Fig. 3(b), the hypothetical field, where SrSi<sub>2</sub> enters the band gap under the assumption of a fixed  $E_F$ , is identified as  $B_{G,\beta}$ .

A specific feature of the quasi-quantized Hall regime in 3D systems is that  $B_{QL}$  and  $\sigma_{xy}$  sensitively depend on the size of the FS in zero field, i.e.,  $k_{F,0,\beta}$  [16,20,21,23]. To test whether our observations, in particular, the onset and  $\sigma_{xy}$  in the 3D QQHI state scale accordingly, we grew an additional batch of SrSi<sub>2</sub> samples with 2% Ca doping, which is known to shift the intrinsic  $E_F$  closer to the valence-band edge [26]. The details of the experiments and analysis of the Ca-doped SrSi<sub>2</sub> samples are provided in Figs. S3–S5 in the Supplemental Material [30]. The results observed for the pure sample are fully reproduced with Ca doping, but they are scaled by a

smaller  $k_{F,0,\beta}$ . This is an important cross-check that reaffirms the occurrence of the 3D QQHI state in SrSi<sub>2</sub>.

In conclusion, we have reported experimental evidence for a quasi-quantized Hall insulator in the lowest Landau band (quantum limit) of the 3D compound SrSi<sub>2</sub>. Our measurements reveal a magnetic-field range in which the longitudinal resistivity diverges with decreasing temperature and the Hall conductivity only depends on the conductance quantum and the Fermi wave vector in the field direction [ $\rho_{xx}(B) \rightarrow \infty$  and  $\sigma_{xy}(B) \rightarrow 6(e^2/h)k_{F,\beta}/\pi$  as  $T \rightarrow 0$ ]. The quasi-quantized Hall insulator is a magnetic field induced insulating ground state of a 3D material that is deeply rooted in quantum physics.

*Acknowledgments.* K.M., N.K., and C.F. acknowledge financial support by the European Research Council (ERC) Advanced Grant No. 742068 (“TOPMAT”). K.M. acknowledges

the Department of Atomic Energy (DAE), Government of India, for the funding support via the Young Scientist’s Research Award (YSRA) via Grant No. 58/20/03/2021-BRNS/37084 and the Max Planck Society for the funding support under the Max Planck–India partner group project. C.F. and J.W. acknowledge support by Deutsche Forschungsgemeinschaft (DFG) under SFB 1143 (Project No. 247310070) and Würzburg-Dresden Cluster of Excellence on Complexity and Topology in Quantum Matter-ct.qmat (EXC 2147, Project No. 39085490). J.W. also acknowledges support from the DFG through the ANR-DFG grant Fermi-NES<sub>t</sub> and by Hochfeld-Magnetlabor Dresden (HLD) at HZDR, member of the European Magnetic Field Laboratory (EMFL). J.G. acknowledges support from the European Union’s Horizon 2020 research and innovation program under Grant Agreement ID 829044 “SCHINES.”

- 
- [1] M. Hilke, D. Shahar, S. H. Song, D. C. Tsui, Y. H. Xie, and D. Monroe, *Nature (London)* **395**, 675 (1998).
- [2] M. Hilke, D. Shahar, S. H. Song, D. C. Tsui, M. Shayegan, and Y. H. Xie, *Ann. Phys.* **8**, 603 (1999).
- [3] M. Hilke, D. Shahar, S. H. Song, D. C. Tsui, Y. H. Xie, and M. Shayegan, *EPL* **46**, 775 (1999).
- [4] D. Shahar, D. C. Tsui, M. Shayegan, J. E. Cunningham, E. Shimshoni, and S. L. Sondhi, *Solid State Commun.* **102**, 817 (1997).
- [5] D. Shahar, D. C. Tsui, M. Shayegan, E. Shimshoni, and S. L. Sondhi, *Phys. Rev. Lett.* **79**, 479 (1997).
- [6] A. de Visser, L. A. Ponomarenko, G. Galistu, D. T. N. de Lang, A. M. M. Pruisken, U. Zeitler, and D. Maude, *J. Phys.: Conf. Ser.* **51**, 379 (2006).
- [7] D. T. N. de Lang, L. A. Ponomarenko, A. de Visser, and A. M. M. Pruisken, *Phys. Rev. B* **75**, 035313 (2007).
- [8] R. Levy and Y. Meir, [arXiv:1005.5245](https://arxiv.org/abs/1005.5245).
- [9] E. Shimshoni and A. Auerbach, *Phys. Rev. B* **55**, 9817 (1997).
- [10] L. P. Pryadko and K. Chaltikian, *Phys. Rev. Lett.* **80**, 584 (1998).
- [11] D. Shahar, D. C. Tsui, M. Shayegan, E. Shimshoni, and S. L. Sondhi, *Science* **274**, 589 (1996).
- [12] E. Shimshoni, S. L. Sondhi, and D. Shahar, *Phys. Rev. B* **55**, 13730 (1997).
- [13] K. V. Klitzing, G. Dorda, and M. Pepper, *Phys. Rev. Lett.* **45**, 494 (1980).
- [14] K. von Klitzing, T. Chakraborty, P. Kim, V. Madhavan, X. Dai, J. McIver, Y. Tokura, L. Savary, D. Smirnova, A. Rey, C. Felser, J. Gooth, and X. Qi, *Nat. Rev. Phys.* **2**, 397 (2020).
- [15] S. Kivelson, D.-H. Lee, and S.-C. Zhang, *Phys. Rev. B* **46**, 2223 (1992).
- [16] J. Noky, J. Gooth, Y. Sun, and C. Felser, *J. Phys. Commun.* **5**, 45007 (2021).
- [17] H. Sakai, H. Fujimura, S. Sakuragi, M. Ochi, R. Kurihara, A. Miyake, M. Tokunaga, T. Kojima, D. Hashizume, T. Muro, K. Kuroda, T. Kondo, T. Kida, M. Hagiwara, K. Kuroki, M. Kondo, K. Tsuruda, H. Murakawa, and N. Hanasaki, *Phys. Rev. B* **101**, 081104(R) (2020).
- [18] H. Masuda, H. Sakai, M. Tokunaga, Y. Yamasaki, A. Miyake, J. Shiogai, S. Nakamura, S. Awaji, A. Tsukazaki, H. Nakao, Y. Murakami, T. Arima, Y. Tokura, and S. Ishiwata, *Sci. Adv.* **2**, e1501117 (2016).
- [19] F. Tang, Y. Ren, P. Wang, R. Zhong, J. Schneeloch, S. A. Yang, K. Yang, P. A. Lee, G. Gu, Z. Qiao *et al.*, *Nature (London)* **569**, 537 (2019).
- [20] S. Galeski, T. Ehmcke, R. Wawrzyńczak, P. M. Lozano, K. Cho, A. Sharma, S. Das, F. Küster, P. Sessi, M. Brando, R. Küchler, A. Markou, M. König, P. Swekis, C. Felser, Y. Sassa, Q. Li, G. Gu, M. V. Zimmermann, O. Ivashko *et al.*, *Nat. Commun.* **12**, 3197 (2021).
- [21] S. Galeski, X. Zhao, R. Wawrzyńczak, T. Meng, T. Förster, P. M. Lozano, S. Honnali, N. Lamba, T. Ehmcke, A. Markou, Q. Li, G. Gu, W. Zhu, J. Wosnitza, C. Felser, G. F. Chen, and J. Gooth, *Nat. Commun.* **11**, 5926 (2020).
- [22] P. Wang, Y. Ren, F. Tang, P. Wang, T. Hou, H. Zeng, L. Zhang, and Z. Qiao, *Phys. Rev. B* **101**, 161201(R) (2020).
- [23] R. Wawrzyńczak, S. Galeski, J. Noky, Y. Sun, C. Felser, and J. Gooth, *Sci. Reports* **12**, 2153 (2022).
- [24] S.-M. Huang, S. Y. Xu, I. Belopolski, C.-C. Lee, G. Chang, T.-R. Chang, B. Wang, N. Alidoust, G. Bian, M. Neupane *et al.*, *Proc. Natl. Acad. Sci. USA* **113**, 1180 (2016).
- [25] B. Singh, G. Chang, T.-R. Chang, S.-M. Huang, C. Su, M.-C. Lin, H. Lin, and A. Bansil, *Sci. Rep.* **8**, 10540 (2018).
- [26] M.-Y. Yao, J. Noky, K. Manna, N. Kumar, V. N. Strocov, C. Shekhar, Y. Sun, and C. Felser, [arXiv:2106.11332](https://arxiv.org/abs/2106.11332).
- [27] G. Kresse and J. Furthmüller, *Phys. Rev. B* **54**, 11169 (1996).
- [28] J. Heyd, G. E. Scuseria, and M. Ernzerhof, *J. Chem. Phys.* **118**, 8207 (2003).
- [29] A. A. Mostofi, J. R. Yates, Y.-S. Lee, I. Souza, D. Vanderbilt, and N. Marzari, *Comput. Phys. Commun.* **178**, 685 (2008).
- [30] See Supplemental Material at <http://link.aps.org/supplemental/10.1103/PhysRevB.106.L041113> for further detailed method of single-crystal growth, ARPES measurements, analysis of Hall measurements, and Shubnikov–de Haas oscillations.
- [31] V. N. Strocov, T. Schmitt, U. Flechsig, T. Schmidt, A. Imhof, Q. Chen, J. Raabe, R. Betemps, D. Zimoch, J. Krempasky, X. Wang, M. Grioni, A. Piazzalunga, and L. Patthey, *J. Synchrotron Radiat.* **17**, 631 (2010).

- [32] V. N. Strocov, X. Wang, M. Shi, M. Kobayashi, J. Krempasky, C. Hess, T. Schmitt, and L. Patthey, *J. Synchrotron Radiat.* **21**, 32 (2014).
- [33] Topological\_Material\_Database, <https://www.topologicalquantumchemistry.com/#/>.
- [34] D. Shoenberg, *Magnetic Oscillations in Metals* (Cambridge University Press, Cambridge, 1984).
- [35] Y. G. Arapov, S. V. Gudina, E. V. Deryushkina, N. G. Shelushinina, and M. V. Yakunin, *Low Temp. Phys.* **45**, 181 (2019).
- [36] S. A. Trugman, *Phys. Rev. B* **27**, 7539 (1983).
- [37] J. T. Chalker and P. D. Coddington, *J. Phys. C: Solid State Phys.* **21**, 2665 (1988).
- [38] J. T. Chalker, *Supersymmetry and Trace Formulae, Chaos and Disorder* (Springer, Berlin, 1999), p. 75.
- [39] J. T. Chalker and A. Dohmen, *Phys. Rev. Lett.* **75**, 4496 (1995).
- [40] L. P. Pryadko and A. Auerbach, *Phys. Rev. Lett.* **82**, 1253 (1999).
- [41] U. Zülicke and E. Shimshoni, *Phys. Rev. B* **63**, 241301(R) (2001).